Journal of Engineering Science and Technology
Vol. 13, No. 11 (2018) 3532 - 3546

COMPARATIVE ANALYSES FOR RCS OF 10 GHz PATCH ANTENNA USING SHORTED STUBS METAMATERIAL ABSORBER

DHAWAN SINGH*, VIRANJAY M. SRIVASTAVA

Department of Electronic Engineering, Howard College,
University of KwaZulu-Natal, Durban - 4041, South Africa
*Corresponding Author: dhawan_deor@ieee.org

Abstract

In this research work, a novel approach for the in-band reduction of Radar Cross Section (RCS) of rectangular patch antenna has been proposed. An ultrathin Metamaterial Absorber (MMA) consists of shorted stubs and rectangular bars has been loaded around the patch antenna. The referenced patch antenna and MMA are designed at the same central frequency of 10 GHz corresponds to X-band. Three different MMA loaded rectangular patch antenna designs are proposed and their behaviours are simulated, analysed and measured. Compared with the conventional patch antenna, the analysis shows that lower RCS values achieved as the number of MMA layers increase around the existing source. At 10 GHz, the maximum monostatic RCS reduction of 9.61 dBsm, 22.67 dBsm and 23.68 dBsm have been achieved for Design 1, Design 2 and Design 3 respectively. While the antenna characteristics and radiation performances almost remain unaffected and preserved.

Keywords: Metamaterial absorber, Monostatic and bistatic, Patch antenna, Radar cross section, X-band.

1. Introduction

Recently, the design of Metamaterial Absorbers (MMA) with near-unity absorbance has been designed and proposed ranging in the microwave regime, THz, infrared and visible light [1-4]. As stated by Ghosh et al. [5] and Singh and Srivastava [6], it offers characteristics like ultra-thin, wide angle of incidence [7], and highly polarization insensitive [8]. It can be a single to wide-band, double-band and multi-band [9-12]. Thus, make it suitable for several intended applications such as antenna designs [13], solar and thermo-photovoltaic cells to improve the performance by enhancing absorption [14, 15], for the reduction of RCS in stealth technology [16-19] and in wireless communication [20, 21].

The RCS of any physical object is directly related to the reflected part of the incidence Electromagnetic (EM) wave and it is determined by the body shape, size and constituent material of the objects. According to Liu et al. [22], in the military platform for communication, the antenna is one of the indispensable instruments that are more susceptible and main contributor for RCS. Without compromising radiation performances, the reduction of RCS for the antenna has been a topic of immense interest. Based on studies by Joozdani et al. [23] and Li et al. [25], for out-band Frequency Selective Surface (FSS), Electronic Band Gap (EBG) structure and Artificial Magnetic Conductor (AMC) structures have been employed for reduction of RCS of the antenna. However, for in-band frequency, it becomes comparatively difficult to reduce the RCS of the antenna [9, 26]. In this research work, a circular MMA structure composed of shorted stubs and rectangular bars has been utilized to enhance the in-band stealth capability of patch antenna operating at 10 GHz.

A comparative design principle has been adopted to study and analyze the performance of MMA absorber, which is placed around the patch antenna. The results show a significant reduction in monostatic as well bistatic RCS of patch antenna while preserving its radiation performance. This research work has been organized as follow: Section 2 explains the design principles of the shorted stubs MMA. Section 3 describes the design principle and analysis of patch antenna with and without MMA. In Section 4, the monostatic and bistatic RCS response of antenna has been analysed and tested. Finally, the work has been concluded and the future directions are recommended in Section 5.

2. Design Principle and Analysis of Shorted Stubs MMA

The proposed MMA design is composed of a circular ring with shorted stubs and rectangular bar that acts as a bandstop resonator. It specifically stops the surface wave propagation between rectangular patch antennas operating at 10 GHz. Due to the high decoupling efficiency and almost unity absorbance, the proposed structure not only degrades the mutual coupling effect but also reduce the in-band RCS of the antenna.

A perfect MMA design must be simple, controllable and highly insensitive for oblique angle of incidence and polarizations to the impinged EM wave. The expression of absorbance is presented, as:

$$A(\omega) = 1 - T(\omega) - R(\omega) \quad (1)$$

where $A(\omega)$, $T(\omega)$ and $R(\omega)$ are the absorbance, transmission and reflection spectrum with the function of frequency ω respectively [27, 28]. For absorbance to reach unity, the value of $T(\omega)$ and $R(\omega)$ should be minimum. Because of the back metallic copper layer, the value of $T(\omega)$ reduces to zero. So, Eq. (1) is modified to:

$$A(\omega) = 1 - R(\omega) \tag{2}$$

This is possible if the impedance of the MMA matched to that of free space impedance. This is achieved by varying geometrical structural parameters. As explained by Smith et al. [29] and Ghosh et al. [30] at one frequency, this value of $R(\omega)$ reduces to zero that corresponds to unity absorbance. In simulations, the thickness of the MMA layer and ground metal plane is 35 µm. The design of circular MMA with concentric loops and shorted stubs has been proposed and analysed. The geometry of the MMA unit cell with all its parameters values has been shown in Fig. 1. The front view and side view of MMA unit cells have been given in Figs. 1(a) and (b), while its frequency response peaks for absorbance, reflectance, and transmittance have been depicted in Fig. 1(c) and the TE mode polarization sensitive behaviour has been analysed in Fig. 1(d), respectively.

The MMA is designed to operate at 10 GHz in X-band by optimizing and adjusting the thickness of the substrate, the radius of the circle, the length of the shorted stubs and rectangular bars. An absorbance of 99.95 % has been achieved at 10 GHz and that approximates to unity absorbance. This MMA operates at wide operating angles where absorbance remained above 94 % for θ (0^0 to 50^0). For θ =70^0 it becomes 72.58%. Since this structure possesses symmetry property so TM mode analysis of EM wave has not considered for this research work.

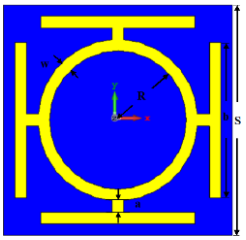

(a) Front view.

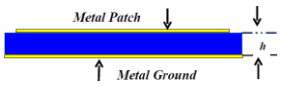

(b) Side view.

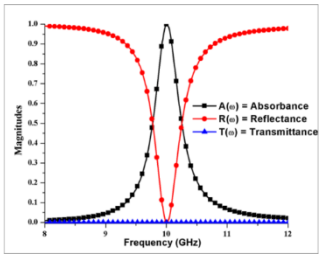

(c) Curves for A(ω), R(ω) and T(ω).

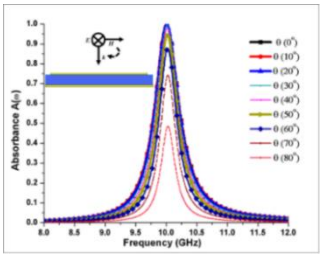

(d) Oblique angle of incidence (θ).

Fig. 1. Metamaterial absorber unit cell dimensions: *S* = 5 mm, *R* = 1.5 mm, *a* = *w* = 0.25 mm, *h* = 0.40 mm.

3. Design Principle and Analysis of Patch Antenna with and without MMA

A microstrip antenna also called patch antenna are becoming very popular antennas in the microwave frequency range because of its simplicity, linearly polarized, conformability to planar and non-planar structures, cost-effective, ease of implementation and compatible with the circuit board technology [31-33]. Based on studies by Balanis [34] and Jang et al. [35], the following general equations have been used to calculate the length (L_s) and width (W_s) of the patch antenna:

$$\Delta L = 0.412 \frac{(\varepsilon_{reff}+0.3)\left(\frac{W_s}{h_1}+0.264\right)}{(\varepsilon_{reff}-0.258)\left(\frac{W_s}{h_1}+0.8\right)} h_1 \tag{3}$$

The effective length of the patch becomes:

$$L_s = L_{eff} - 2\Delta L \tag{4}$$

The effective length (L_{eff}), for resonant frequency (f_0), is given as:

$$L_{eff} = \frac{c}{2f_0\sqrt{\varepsilon_{reff}}} \tag{5}$$

and

$$\varepsilon_{eff} = \frac{\varepsilon_r+1}{2} + \frac{\varepsilon_r-1}{2}\left[1 + 12\frac{h_1}{W_s}\right]^{-\frac{1}{2}} \tag{6}$$

The resonance frequency corresponds to any TM_{mn} mode is given as:

$$f_0 = \frac{c}{2\sqrt{\varepsilon_{reff}}}\left[\left(\frac{m}{L_s}\right)^2 + \left(\frac{n}{W_s}\right)^2\right]^{1/2} \tag{7}$$

Here, m and n are modes with respect to L_s and W_s respectively. For resonance, the width is given as:

$$W_s = \frac{c}{2f_0\sqrt{\frac{\varepsilon_r+1}{2}}} \tag{8}$$

The top layer is the radiating patch made up of copper-backed by a most popular, low cost and readily available flame retardant FR4 substrate with the loss tangent value is 0.025 and ε_r is 4.3. The ground layer is made up of copper. The length of the radiating patch (L) is 6.50 mm and the length of the central substrate (L_1) is 15 mm whereas the central thickness of the substrate (h_1) is 1 mm. The thickness of the area (h) around exiting source is 0.4 mm, which is compatible and specifically designed to load ultra-thin MMA absorbers for unity absorbance.

All the parameters are optimized to resonant at 10 GHz and their tabular description has been given in Table 1. Each design has been fed by coaxial feed with its central approximates to 50 Ω matching the impedance at the position, pos_x =1.25 mm and pos_y = 0 as shown in Fig. 2. Coaxial feed technique has been adopted for our research work because of its simplicity and uncomplicated impedance matching characteristics. The outer conducting layer of the SMA connector is connected to the ground plane, while the centre conductor is fed through the substrate and ground-plane by drilling hole and electrically connected to the patch antenna. To minimize the mutual coupling and keep the antenna radiation performance unaffected a small gap (g_s) of 3.5 mm has been left between MMA and each design.

Table 1. Antenna parameter description.

Description	Dimensions (mm)	Parameters
L_s/W_s	35/55/75	Periodicity of structure
L_1	15	Central substrate length
h_1	1	Height of substrate
L	6.50	Length of patch
g_s	3.5	Gap b/w patch and MMA
t	0.035	Thickness of metal
Pos_*x*	1.25	Position of probe
h_0	5	Height of connector

The complete research work has been divided into three design models to evaluate the possibility and capability of MMA structure in enhancing the stealth capability along with to study the effects of MMA on patch antenna radiation performance. In Design 1, initially, a referenced patch antenna of periodicity 35 mm × 35 mm is designed with and without two MMA layers and its radiation performance is simulated and analysed as depicted in Fig. 2.

This referenced patch antenna is then modified and extended to four layers of MMA in Design 2 with the periodicity of 55 mm × 55 mm as shown in Fig. 3. Finally, this structure is further extended in Design 3, where the exiting source is loaded with six layers of MMA structure with the periodicity of 75 mm × 75 mm as depicted in Fig. 4. All designs are fabricated and measured with and without MMA structure. It has been obtained that as we start increasing the number of MMA layers around exiting source the resonant frequency (f_0) response remains almost unaffected. To study the effect of MMA structure on patch antenna radiation performances, comparative analyses have been made and being tabularized in Table 2.

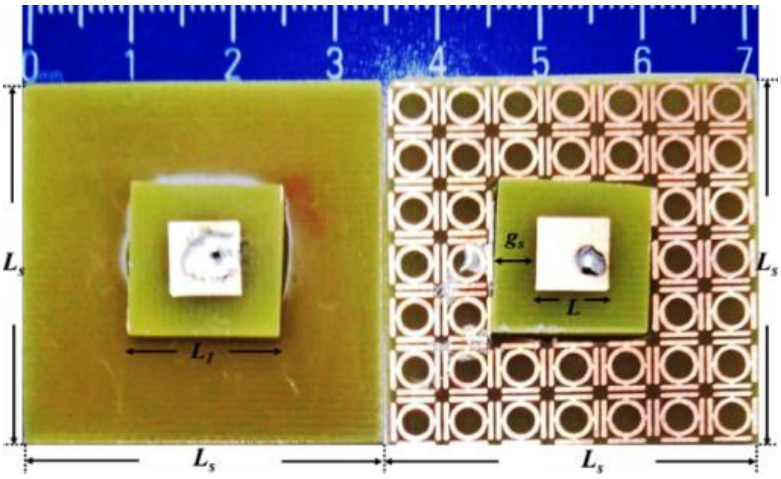

(a) Referenced antenna. (b) MMA loaded antenna.

Fig. 2. Coaxial feed Patch Antenna 35 mm × 35 mm Design 1.

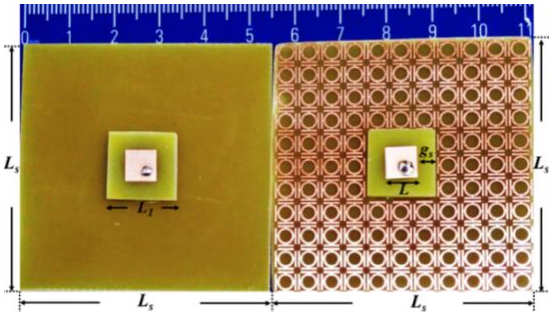

(a) Referenced antenna. (b) MMA loaded antenna.

Fig. 3. Coaxial feed Patch Antenna 55 mm × 55 mm Design 2.

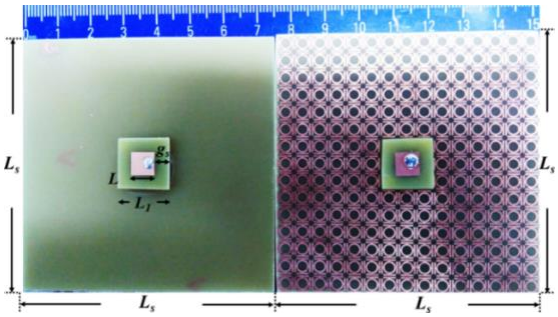

(a) Referenced antenna. (b) MMA loaded antenna.

Fig. 4. Coaxial feed Patch Antenna 75 mm × 75 mm Design 3.

Table 2. Antenna radiation performance comparison.

Structure/ performance parameters	Design 1		Design 2		Design 3	
	Referenced antennna	MMA modified antenna	Referenced antenna	MMA modified antenna	Referenced antenna	MMA modified antenna
Size	35 mm × 35 mm		55 mm × 55 mm		75 mm × 75 mm	
f_0 **(GHz)**	10	9.96	10.01	9.98	10	9.99
S_{11} **(dB)**	-48.17	-44.39	-35.45	-35.62	-34.49	-38.49
BW (MHz)	456	460	468	436	468	460
η	63.02	53.43	64.09	52.06	64.29	51.04
VSWR	1.01	1.14	1.04	1.06	1.04	1.05
Z_{11} **(Ω)**	50.27	46.94	52.03	47.23	51.33	49.60

The radiation performance curves have been analysed and shown in Fig. 5. For Design 1, the referenced antenna achieved resonance at 10 GHz frequency with the scattering coefficient (S_{11}) value of -48.17 dB. Although, after loading with MMA layers its resonance peak slightly moves to 9.96 GHz with S_{11} equal to -44.39 dB. For Design 2, the referenced antenna resonance peak appears at 10.01 GHz frequency with S_{11} value corresponds to -35.45 dB and after loading with MMA layers its resonance slightly shifted to 9.98 GHz with S_{11} value reached -35.62 dB. For Design 3, the referenced antenna resonance remains unaltered to 10 GHz frequency with S_{11} value of -34.49 dB and after loading with MMA layers its resonance slightly shifted to 9.99 GHz with S_{11} value of -38.49 dB as shown in Fig. 5(a).

For Design 1, the value of return loss parameter increases marginally after loading MMA structure. While for Design 2 and 3 after loading MMA layers the values slightly diminished. This behaviour is observed because of a shift in matching impedance (Z_{11}) with the increase in the periodicity of the structure as shown in Fig. 5(b). For Design 1, the shift in Z_{11} for modified patch antenna with respect to 50 Ω matching impedance is 3.06 Ω and for Design 2 it starts reducing and becomes equal to 2.77 Ω. While for Design 3, the value of Z_{11} approaches to 50 Ω matching impedance and reduces as close as 0.4 Ω.

A comparison for -10 dB bandwidth (BW), Voltage Standing Wave Ratio (VSWR) and radiation efficiency (η) between referenced antenna and MMA modified patch antenna for all three designs have been made. The analysis indicates that the bandwidth remains almost unaltered for all design models. The simulated value of VSWR for all design remains within the acceptable range from 1.0 to 2.0 as depicted in Fig. 5(c). Similarly, a simulation analysis has made to find out the efficiency of the antenna and a small reduction in Radiation Efficiency (η) has been observed after loading with MMA and shown in Fig. 5(d). Analyses of directivity and gain between referenced antenna and MMA loaded patch antenna have been made and its polar plots have been drawn in Fig. 6.

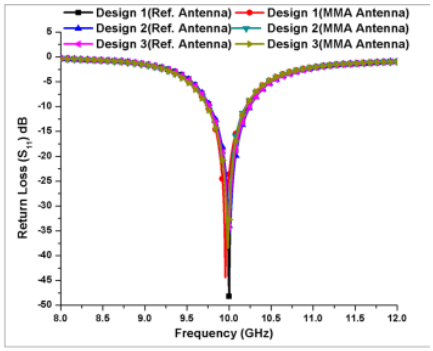

(a) Return loss (S_{11}).

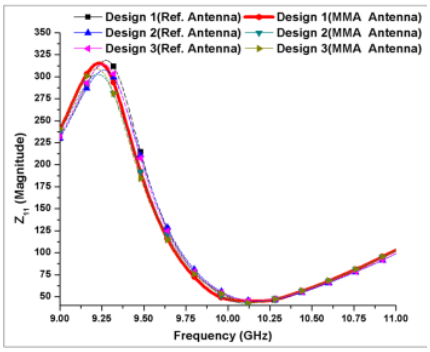

(b) Impedance (Z_{11}).

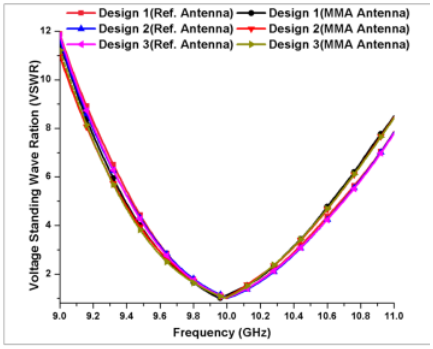

(c) Voltage Standing Wave Ratio (VSWR).

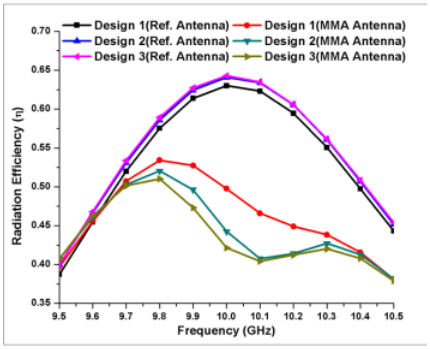

(d) Radiation efficiency (η).

Fig. 5. Comparison of antenna radiation characteristics.

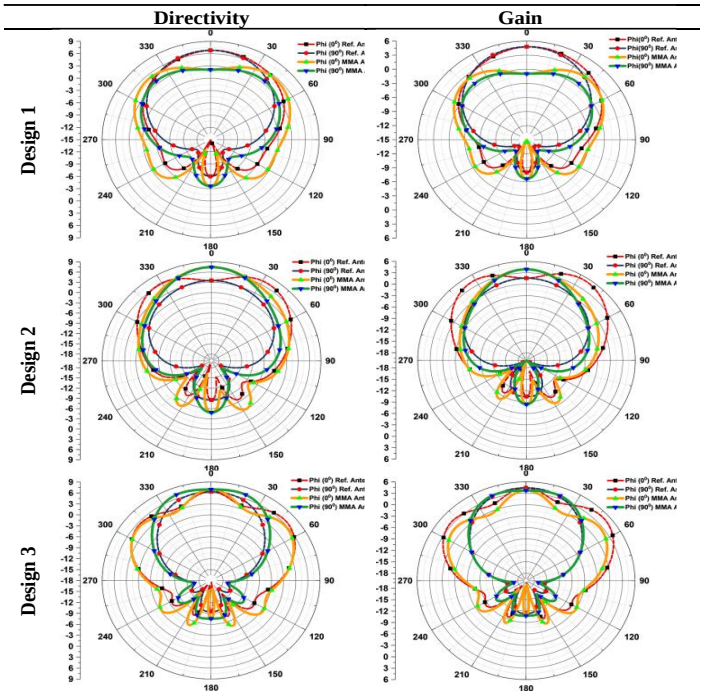

Fig. 6. Comparison of directivity and gain.

In Design 1 for E-Plane, the reference patch main lobe magnitude is 6.83 dBi and for MMA loaded antenna it is reduced to 5.57 dBi. For Design 2, the reference patch antenna main lobe magnitude becomes 7.11 dBi and after loading with MMA it is slightly increased to 7.45 dBi. For Design 3, the referenced patch main lobe magnitude becomes 6.69 dBi and after loading MMA it is increased to 6.96 dBi. In Design 1 for H-Plane, the reference patch main lobe magnitude is 6.79 dBi, while for MMA loaded antenna it is unexpectedly reduced to 3.36 dBi. For Design 2, reference patch main lobe magnitude becomes 3.52 dBi and after loading MMA it is sharply increased to 7.45 dBi. For Design 3, the reference patch main lobe magnitude becomes 6.35 dBi and after loading MMA it is increased to 7.16 dBi. Therefore, the directivity performance for Design 1 remained poor while for Design 2 and 3 its performance increases after loading MMA.

In Design 1 for E-Plane, the reference patch main lobe gain magnitude is 4.82 dB and for MMA loaded antenna it is sharply reduced to 2.54 dB. For Design 2, the reference patch antenna main lobe magnitude becomes 5.17 dB and after loading MMA it is reduced to 3.91 dB. For Design 3, the reference patch main lobe magnitude becomes 4.77 dB and after loading MMA it is also reduced to 3.71 dB. In Design 1 for H-Plane, the reference patch main lobe magnitude is 4.79 dB. while for MMA loaded antenna, it is unexpectedly reduced to 0.632 dB. For Design 2, the reference patch main lobe magnitude becomes 1.59 dB and after loading MMA it is increased to 3.91 dB. For Design 3, the reference patch main lobe magnitude becomes 4.43 dB and after loading MMA it is marginally reduced to 3.91 dB. So, the results show a poor gain performance for Design 1, whereas for Design 2, it is affected marginally and for Design 3 it is remained well kept and tabularized in Table 3.

Table 3. Comparison of antenna directivity and gain for E-Plane and H-Plane.

Structure/performance parameters (10 GHz)		Phi (ϕ)	Directivity (dBi)	Gain (dB)
Design 1	Referenced antenna	0^0	6.83	4.82
		90^0	6.79	4.79
	MMA modified	0^0	5.57	2.54
		90^0	3.66	0.63
Design 2	Referenced antenna	0^0	7.11	5.17
		90^0	3.52	1.59
	MMA modified	0^0	7.45	3.91
		90^0	7.45	3.91
Design 3	Referenced antenna	0^0	6.69	4.77
		90^0	6.35	4.43
	MMA modified	0^0	6.96	3.71
		90^0	7.16	3.91

4. Application of MMA in Patch Antenna for RCS Reduction

As compared to conventional antenna geometry, monostatic RCS of the MMA loaded patch antenna is almost polarization independent. Monostatic RCS of the conventional antenna and MMA loaded patch antenna for *x*-polarization and *y*-polarization incidence waves have been shown with its measured values in Fig. 7.

For Design 1, it has been found that the value for monostatic RCS reduced throughout the observation band after loading it with MMA as shown in Fig. 7(a). At 10 GHz resonant frequency, the reduction in monostatic RCS for MMA loaded antenna is -26.39 dBsm for *x*-polarization and -28.17 dBsm for *y*-polarization. However, the significant peak reduction is obtained at 9.93 GHz with -28.82 dBsm for *x*-polarization and at 9.95 GHz with -30.16 dBsm for *y*-polarization. So, a maximum difference of 9.61 dBsm observed for *x*-polarization and 10.82 dBsm for y-polarization between referenced and proposed antenna.

For Design 2, at 10 GHz resonant frequency, the reduction in monostatic RCS for MMA loaded antenna is -18.32 dBsm for *x*-polarization and -17.90 dBsm for *y*-polarization. Whereas, the significant peak reduction is obtained at 9.91 GHz with -31.89 dBsm and -48.04 dBsm for *x*-polarization and as well for *y*-polarization respectively as shown in Fig. 7(b). A maximum difference of 22.67 dBsm observed for *x*-polarization 38.56 dBsm for *y*-polarization between referenced and proposed antenna.

For Design 3, at 10 GHz resonant frequency the reduction in monostatic RCS for MMA loaded antenna is -11.17 dBsm for *x*-polarization and -10.96 dBsm for *y*-polarization. Although, the significant peak reduction is obtained at 9.89 GHz with -27.39 dBsm and -32.62 dBsm for *x*-polarization as well as for *y*-polarization respectively as depicted in Fig. 7(c). So, a maximum difference of 23.68 dBsm observed for *x*-polarization 28.59 dBsm for *y*-polarization between referenced and proposed antenna. Small deviations in simulated and measured results are found during fabrication, handling and testing of structure and cannot be avoided.

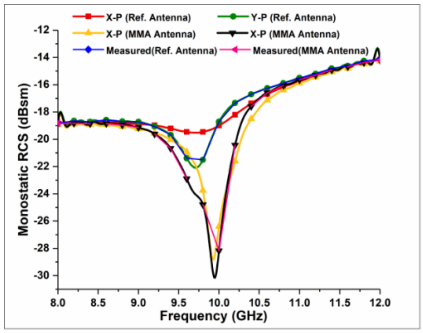

(a) Design 1.

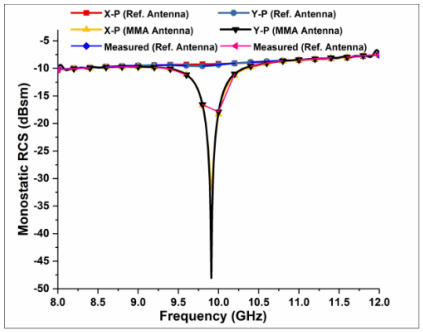

(a) Design 2.

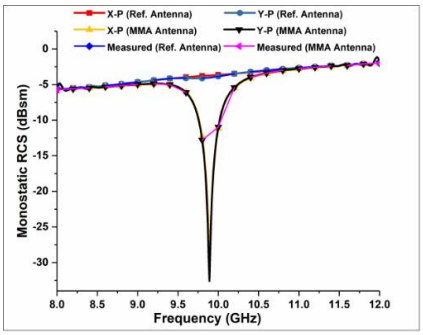

(c) Design 3.

Fig. 7. Comparison of *x*-polarization and *y*-polarization for monostatic RCS.

A simulation analysis of conventional patch antenna and MMA loaded patch antenna has been also made for bistatic RCS of horizontal and vertical polarization as depicted in Fig. 8. The bistatic RCS of the referenced antenna and proposed MMA modified antenna has been simulated and analysed at 10 GHz. Vertical polarization curves for all designs have been also given. Since the structure is almost polarization independent so its behaviours are not considered here. The measured RCS values for antennas are in good agreements with the simulation results. For Design 1 at φ =0 ^{o}, the bistatic RCS of the MMA loaded antenna reduced significantly throughout the angle theta (θ) between -83^{o} to 84^{o}. However, the maximum difference is observed of 36.03 dBsm at 34^{o} and16.40 dBsm at -34^{o}, respectively. At φ = 90 ^{o}, the bistatic RCS of the MMA loaded antenna reduced significantly for theta (θ) with a major reduction in between -144^{o} to 144^{o}. However, the maximum difference is observed of 13.48 dBsm at 50^{o} and -50^{o}, respectively between reference and MMA loaded antenna.

For Design 2 at φ = 0 ^{o}, the bistatic RCS of the MMA loaded antenna reduced significantly throughout the angle theta (θ) between -82^{o} to 82^{o}. However, the maximum difference is observed of 44.17 dBsm at 59^{o} and 33.89 dBsm at -54^{o}, respectively. At φ = 90 ^{o}, the bistatic RCS of the MMA loaded antenna reduced significantly throughout the angle theta (θ) with a major reduction in between -176^{o} to 176^{o}. However, the maximum difference is observed of 13.80 dBsm at 33^{o} and -33^{o}, respectively between reference and MMA loaded antenna.

For Design 3 at φ = 0 ^{o}, the bistatic RCS of the MMA loaded antenna between -81^{o} to 81^{o}. However, the maximum difference is found of 27.96 dBsm at

70º and 28.07 dBsm at -73º, respectively. At φ = 90 º, the bistatic RCS of the MMA loaded antenna reduced significantly throughout the angle theta (θ) with a major reduction in between -169º to 169º. However, the maximum difference is noticed of -13.50 dBsm at 25º and -25º, respectively between the reference and MMA loaded antenna.

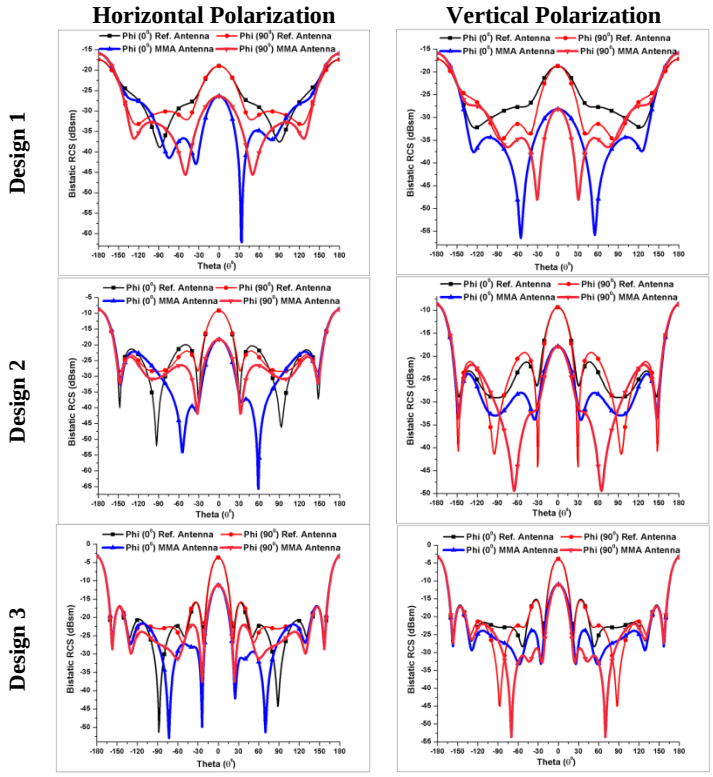

Fig. 8. Comparison of bistatic RCS at 10 GHz.

5. Conclusions

In this research work, a comparative design analysis of MMA loaded patch antenna has been proposed. The results show that monostatic and bistatic RCS of patch antenna has been reduced significantly for all proposed designs. It has been found that as we increase the number of MMA layers around the existing source, the value of RCS reduces simultaneously. For *x*-polarization, the maximum monostatic RCS reduction of 9.61 dBsm, 22.67 dBsm and 23.68 dBsm have been observed for Design 1, Design 2 and Design 3, respectively. While for *y*-polarization, the maximum monostatic RCS reduction of 10.82 dBsm, 38.56 dBsm and 28.59 dBsm have been observed for Design 1, Design 2 and Design 3, respectively. However, with an increase in the periodicity of the designed substrate, it raises issues like complexity in designing, size and additional cost. Therefore, it is a compromise between the periodicity and RCS reduction. It concludes that one can achieve better RCS value by controlling and optimizing the periodicity of the structure. An

analysis has been also made to study the effect of MMA on the patch antenna before and after loading it. The results indicate that the radiation performance of the patch antenna has been affected marginally.

Design 1 shows unsatisfactory directivity and gains response. Whereas, for Design 2 and 3, directivity is enhanced with gain is affected slightly. Therefore, MMA is best suitable for available technology for in-band RCS reduction of antennas, while antenna radiation performance affected slightly. Even though, a single patch antenna design has some limitations and suffers from fringing effects that result in low radiation performance such as narrow bandwidth, lower directivity, gain, radiation efficiency and less power handling capability.

Therefore, it cannot be suitable for long-distance communication, especially for military applications. One of the vital solutions is to combine a few antennas to form a patch array. It has been observed that its overall radiation performance enhances and thus, it could compensate for radiation losses after loading it with MMA structure and this is left for future research work. This work finds its applications in military and stealth platform for lower detectable objects.

Nomenclatures

h1	Thickness of substrate, mm
Leff	Effective length of the patch, mm
Ls	Length of the patch, mm
Ws	Width of the patch, mm

Greek Symbols

$\mathcal{E}r$	Relative permittivity
f0	Resonant frequency
η	Efficiency
θ	Angle of incidence
φ	Polarization angle
Ω	Resistance
ω	Angular frequency

Abbreviations

A(ω)	Absorbance
AMC	Artificial Magnetic Conductor
EBG	Electronic Band Gap
EM	Electromagnetic
FSS	Frequency Selective Surface
MMA	Metamaterial Absorber
R(ω)	Reflectance
RCS	Radar Cross Section
T(ω)	Transmittance
VSWR	Voltage Standing Wave Ratio

References

1. Singh, D.; and Srivastava, V.M. (2017). Triple band regular decagon shaped metamaterial absorber for X-band applications. *Proceedings of the IEEE*

International Conference on Computer Communication and Informatics (ICCCI). Coimbatore, India, 1-4.

2. Astorino, M.D.; Frezza, F.; and Tedeschi, N. (2017). Ultra-thin narrow-band, complementary narrow-band, and dual-band metamaterial absorbers for applications in the THz regime. *Journal of Applied Physics*, 121(6), ID 063103.
3. Dai, S.; Zhao, D.; Li, Q.; and Qui, M. (2013). Double-sided polarization-independent plasmonic absorber at near-infrared region. *Optics Express*, 21(11), 13125-13133.
4. Hedayati, M.K.; Faupel, F.; and Elbahri, M. (2014). Review of plasmonic nanocomposite metamaterial absorber. *Materials (Basel)*, 7(2), 1221-1248.
5. Ghosh, S.; Bhattacharyya, S.; Chaurasiya, D.; and Srivastava, K.V. (2015). An ultrawideband ultrathin metamaterial absorber based on circular split rings. *IEEE Antenna and Wireless Propagation Letters*, 14, 1172-1175.
6. Singh, D.; and Srivastava, V.M. (2016). Metamaterial absorber based on concentric rings with shorted stubs. *Proceedings of the 3rd International Conference on Engineering and Technology (ICET)*. Kemaman, Malaysia, 159-163.
7. Ayop, O.; Rahim, M.K.A.; Murad, N.A.; and Samsuri, N.A. (2014). Polarization insensitive and wide operating angle metamaterial absorber at X-band. *Proceedings of the IEEE Asia-Pacific Conference on Applied Electromagnetics (APACE)*. Johor Bahru, Malaysia, 245-249.
8. Ayop, O.; Rahim, M.K.A.; and Murad, N.A. (2015). Polarization-independent metamaterial absorber for single band and multi-band frequency. *Journal Teknologi*, 77(10), 99-106.
9. Singh, D.; and Srivastava, V.M. (2018). Low radar cross section of patch antenna using shorted stubs metamaterial absorber. *International Journal of Microwave and Optical Technology*, 13(3), 194-202.
10. Unal, E.; Bagmanci, M.; Karaaslan, M.; Akgol, O; Arat, H.T.; and Sabah, C. (2017). Zinc oxide-tungsten-based pyramids in construction of ultra-broadband metamaterial absorber for solar energy harvesting. *IET Optoelectronics*, 11(3), 114-120.
11. Singh, D.; and Srivastava, V.M. (2018). Dual resonances shorted stub circular rings metamaterial absorber. *International Journal of Electronics and Communications*, 83, 58-66.
12. Chaurasiya, D.; Ghosh, S.; Bhattacharyya, S.; Bhattacharyya, A; and Srivastava, K.V. (2016). Compact multi-band polarisation-insensitive metamaterial absorber. *IET-Microwaves, Antennas & Propagation*, 10(1), 94-101.
13. Mu, J.; Wang, H.; Wang, H.; and Huang, Y. (2017). Low-RCS and gain enhancement design of a novel partially reflecting and absorbing surface antenna. *IEEE Antenna and Wireless Propagation Letters*, 16, 1903-1906.
14. Li, W.; and Valentine, J. (2014). Metamaterial perfect absorber based hot electron photodetection. *Nano Letters*, 14(6), 3510-3514.
15. Agarwal, S.; and Prajapati, Y.K. (2017). Analysis of metamaterial-based absorber for thermo-photovoltaic cell applications. *IET Optoelectronics*, 11(5), 208-212.

16. Zheng, Y.J.; Gao, J.; Zhou, Y.-L.; Cao, X.-Y.; Xu, L.-M.; Li, S.-J.; and Yang, H.-H. (2017). Metamaterial-based patch antenna with wideband RCS reduction and gain enhancement using improved loading method. *IET Microwaves, Antennas & Propagation*, 11(9), 1183-1189.
17. Li, S.-J.; Gao, J.; Cao, X.-Y.; Zhao, Y.; Zhang. Z.; and Liu, H.-X. (2015). Loading metamaterial perfect absorber method for in-band radar cross section reduction based on the surface current distribution of array antennas. *IET Microwaves, Antennas & Propagation*, 9(5), 399-406.
18. Li, S.; Cao, X.; Liu, T.; and Yang, H. (2014). Double-layer perfect metamaterial absorber and its application for RCS reduction of antenna. *Radio Engineering*, 23(1), 222-228.
19. Zhang, H.; Cao, X.-Y.; Jun Gao, J.; Yang, H.-H.; and Yang, Q. (2014). A novel dual-band metamaterial absorber and its application for microstrip antenna. *Progress in Electromagnetics Research Letters*, 44, 35-41.
20. Shater, A.; and Zarifi, D. (2017). Radar cross section reduction of microstrip antenna using dual-band metamaterial absorber. *Aces Journal*, 32(2), 135-140.
21. Singh, D.; and Srivastava, V.M. (2018). Design implementation of concentric loops with stubs metamaterial absorber. *Wireless Personal Communications*, 1-20.
22. Liu, Y.; Wang, H.; Jia, Y.; and Gong, S. (2014). Broadband radar cross-section reduction for microstrip patch antenna based on hybrid AMC structures. *Progress in Electromagnetics Research C*, 50, 21-28.
23. Joozdani, M.Z.; Amirhosseini, M.K.; and Abdolali, A. (2016). Wideband radar cross-section reduction of patch array antenna with miniaturized hexagonal loop frequency selective surface. *Electronics Letters*, 52(9), 767-768.
24. He, W.; Jin, R.; and Geng, J. (2007). Low radar cross-section and high performances of microstrip antenna using fractal uniplanar compact electromagnetic bandgap ground. *IET Microwaves, Antennas & Propagation*, 1(5), 986-991.
25. Li, W.-Q.; Cao, X.-Y.; Gao, J.; Zhang, Z.; and Cong, L.-L. (2016). Broadband RCS reduction and gain enhancement microstrip antenna using shared aperture artificial composite material based on quasi-fractal tree. *IET Microwaves, Antennas & Propagation*, 10(4), 370-377.
26. Singh, D.; and Srivastava, V.M. (2018). An analysis of RCS for dual-band slotted patch antenna with a thin dielectric using shorted stubs metamaterial absorber. *International Journal of Electronics and Communication*, 90, 53-62.
27. Liu, W. (2015). The study status and development of metamaterial absorber. *Proceedings of the International Conference on Logistics, Engineering, Management and Computer Sci*ence (LEMCS). Shenyang, China, 1318-1322.
28. Soheilifar, M.R.; and Sadeghzadeh, R.A. (2015). Design, fabrication, and characterisation of scaled and stacked layers planar metamaterial absorber. *IET Microwaves, Antennas & Propagation*, 9(1), 86-93.
29. Smith, D.R.; Vier, D.C.; Koschny, T.H.; and Soukoulis, C.M. (2005). Electromagnetic parameter retrieval from inhomogeneous metamaterials. *Physical Review E*, 71(3), 11 pages.

30. Ghosh, S.; Bhattacharyya, S.; Chaurasiya, D.; and Srivastava, K.V. (2015). An ultrawideband ultrathin metamaterial absorber based on circular split rings. *IEEE Antenna and Wireless Propagation Letters*, 14, 1172-1175.
31. Baskey, H.B.; Jha, A.K.; and Akhtar, M.J. (2014). Design of metamaterial based structure for the radar cross section reduction of a microstrip antenna. *Proceedings of the IEEE International Microwave & RF Conference (ImaRC).* Bangalore, India, 104-107.
32. Zhang, Z.-X.; and Zhang, J.-C. (2016). RCS reduction for patch antenna based on metamaterial absorber. *Proceedings of the Progress in Electromagnetic Research Symposium*. Shanghai, China, 364-368.
33. Cong, L.-L.; Cao, X.-Y.; Li, W.-Q.; and Zhao, Y. (2016). A new design method for patch antenna with low RCS and high gain performance. *Progress in Electromagnetics Research Letters*, 59, 77-84.
34. Balanis, C.A. (2005). *Antenna theory: analysis and design* (3rd ed.). Hoboken, New Jersey: John Wiley and Sons Inc.
35. Jang, H.-K.; Shin, J.-H.; and Kim, C.-G. (2010). Low RCS patch array antenna with electromagnetic bandgap using a conducting polymer. *Proceedings of the IEEE International Conference in Electromagnetics Advanced Applications*. Sydney, New South Wales, Australia, 140-143.